



Elastic (acrylate/polydimethylsiloxane) substrate-to-coating interlayers for improving the mechanical resilience of thermoelectric films on poly (ethylene terephthalate) during roll-to-roll manufacture and in service operation

Xudong Tao, Kai Zhang, Bryan W. Stuart, Hazel E. Assender^{*}

Department of Materials, University of Oxford, Parks Road, OX1 3PH, UK

ARTICLE INFO

Keywords:

Flexible/wearable/stretchable electronics
Roll-to-roll manufacture
Bismuth telluride thermoelectrics
Polymer substrate
Mechanical resilience

ABSTRACT

Strain-induced failure is a major concern in wearable electronics. Herein, a ~ 90 -nm thick bismuth telluride film is fabricated on 125- μm thick polyethylene terephthalate as the basis for a flexible thermoelectric generator. To simulate induced mechanical strains during wearable operation and roll-to-roll manufacture, both tensile and buckling strains are studied. To improve the mechanical resilience, two types of substrate-to-coating interlayers with varying thicknesses are investigated: 0.4–7.7 μm -thick Poly-tripropylene glycol diacrylate (acrylate) and 2.5–16.8 μm -thick Poly-dimethyl siloxane (PDMS). The thermoelectric performance of the coating is influenced through the stress, applied on the polymer substrate, being transferred through to the coating. Samples exposed to tensile testing recover once the load is released, mitigating against change on the film morphology and thermoelectric performance, in contrast to those measured in-situ under buckling strain. Both interlayers are shown to assist in maintaining the film performance, as fewer cracks are formed in the semiconductor. A thicker interlayer is shown to better mitigate the impact of deformation of the substrate. Furthermore, in fatigue-bending tests, the film grown on a PDMS interlayer shows better cyclical fatigue performance.

1. Introduction

Flexible thermoelectric generators (TEGs) with stretchability and bendability have attracted increasing attention as green and local power sources for use in wearable electronics [1]. Various architectures have been proposed, but one simple example would have TEG elements in the plane of a film bonded to the skin in which one end only has good thermal contact to the skin, hence setting up a thermal gradient along the TE strips. Flexible TEGs that can conform to the changing curvatures of the human body would require sufficient mechanical compliance and it has been suggested that TEGs would need to accommodate $\sim 1\%$ strain without significant degradation in their electronic performance [2]. Flexible TEGs have mainly been developed in one of two architectures: flexible substrate-bonded materials (e.g. TEGs coated on polymer sheets [3] or textiles [4]) or freestanding conductive materials (e.g. conductive polymer-based TEGs [5] and those based on polymer composites [6]). The novel composite materials have been designed with mechanical properties as a primary factor in the materials design [1,7], but the TE

properties are not as good as might be achieved with thin-film TEGs based on inorganic materials. When considering the more conventional TE materials deposited as thin films on flexible substrates, the flexibility has only rarely been reported, perhaps due to concerns around the inherent brittleness of inorganic thermoelectric (TE) materials such as bismuth telluride (Bi—Te).

Few papers have reported the mechanical properties of Bi—Te thin films grown on flexible polymer substrates. Zhang et al. [8] reported an analytical method to investigate the crack formation in inorganic TE materials (without substrates) and found that the crack size affected the electrical and thermal conductivities whilst showing that the TE conversion efficiency was independent of the crack size. Liu et al. [9] also used modelling to examine the TE behaviour of films grown on a polymer substrate, and they concluded that the film thickness significantly affected the stress level of films. To date, there are few research reports about the experimental observation of mechanical behaviours of TE thin films on polymer substrates. Cao et al. [10] carried out an experimental study of bending properties for a screen-printed TE coating (70–250 μm

^{*} Corresponding author.

E-mail address: hazel.assender@materials.ox.ac.uk (H.E. Assender).

<https://doi.org/10.1016/j.surfcoat.2022.128167>

Received 2 December 2021; Received in revised form 21 January 2022; Accepted 22 January 2022

Available online 29 January 2022

0257-8972/© 2022 The Authors. Published by Elsevier B.V. This is an open access article under the CC BY license (<http://creativecommons.org/licenses/by/4.0/>).

thick Bi—Te and Sb—Te) on textile by flexing the sample at a fixed bend radius over a roller. They observed that the compressive bending effect (over ten bending cycles passing a 60 mm diameter roller and a 4-mm diameter roller) increased the sheet resistance of the TE materials by 200%, and also they observed a debonding phenomenon. Singkaselit et al. [11] reported that annealing could improve the hardness of ~ 1.5 μm thick TE films on polyimide sheets due to a change in the film density. Kong et al. [12] recently reported that coating a polydimethylsiloxane (PDMS) layer on the Bi—Te surface (grown on a polyimide sheet) could significantly improve the resilience of the film. They observed <5% change in resistance after bending 2000 cycles (radius: 7 mm).

In addition to the mechanical forces applied during operation, the mechanics during TEG manufacture is another aspect to consider. In roll-to-roll (R2R) processing, a polymer web unwinds from a winding roller, travels onto a drum where active coating materials are deposited, and rewinds onto a rewinding roller. This is to say, the polymer web undergoes a series of rollers (typically with a core radius of ~ 15 cm) and a coating drum (of typically larger radius, in our case ~ 28 cm), leading to bending of the polymer web and thus the compression/tension in the coating. Besides, in an R2R process, a fixed tension is applied to the polymer web to keep it tight. These factors apply stresses (and hence strains) to the substrate and coating. Typically, the tension could be around 85 N between two rollers (e.g. in the Aerre Machines Vacuum R2R web coater used in this study), corresponding to ~ 24 N/mm² stress for a polymer web (polyethylene terephthalate, PET: 0.125 mm thick and 35 cm wide), which given the modulus of the material corresponds to $\sim 1\%$ strain. The estimated induced strain has been shown to affect the TE properties of organic TE materials [1], so it is likely that the strain also has an effect on the electrical performance of inorganic TE materials on polymer sheets, as also observed for metal thin-films (Ti, Ni, Cr and Au) on polymer PDMS substrates [13].

To improve the mechanical resilience of the TE film grown on polymer substrates, coating a PDMS layer on top of the TE film has been found to be effective (Kong et al. 2019 [12]). However, this method fabricates the PDMS coating after the deposition of TE films on polymer substrates, so it does not solve the induced strain in TE films during the process of R2R manufacture. Therefore, a further study to put a PDMS layer before depositing TE films on the polymer substrate is worth considering. In addition to PDMS, an R2R manufacturable acrylate coating is also explored in this study, as an interlayer in between the PET substrate and the functional film, expected to help improve the mechanical resilience of the functional materials during R2R processing and wearable operation.

Although the mechanical behaviour of polymer substrate-bonded TE materials is not well assessed, such studies on stretchable electronics (e.g. the piezoelectric film [14,15]) have been extensively investigated for several decades, hence similar experimental methods are used in this study. This study aims to investigate the impact of mechanical deformation on TE performance of polymer substrate-bonded inorganic TE thin film materials, and to explore the way of improving their mechanical resilience by putting an interlayer in between the polymer substrate and the functional coating, in-use of wearable TEGs and especially during the R2R manufacturing process such as might be used for the large-scale manufacture of flexible in-plane TEGs [16]).

2. Experimental details

2.1. Sample fabrication

Two types of interlayers (acrylate and PDMS) were deposited onto the PET substrate before Bi—Te deposition for comparison with Bi—Te directly on a blank PET substrate (~ 0.125 mm, Melinex®). As shown in Fig. S1 a, the acrylate layer [17] was made by tripropyleneglycol diacrylate monomer (TPGDA, Sigma—Aldrich) injected into a hot tank (preheated at ~ 240 °C, for 3–6 min according to the amount of TPDGA

monomer (0.6–10 mL), under an injection rate of ~ 0.5 mL/min) and then vacuum-flash evaporated ($\sim 1.8 \times 10^{-4}$ mbar) through nozzles (preheated at ~ 270 °C) onto a PET substrate (rotating under an in-line speed of ~ 25 m/min), followed by an in situ polymerised cure by a 1-min exposure to an Ar plasma (270 V, 5.8 A). By varying the amount of TPGDA injected, a series of acrylate interlayers with different thicknesses were coated onto PET substrates.

A PDMS layer was made using a spin coater (Laurell Technologies Corporation). Similar as in reference [18], PDMS and curing agent (SYLGARD® 184) were mixed in ratio 10:1 and stirred for ~ 5 mins and under vacuum ($\sim 4 \times 10^{-2}$ mbar) for ~ 1 h to degas the mixture. Sufficient PDMS mixture (~ 200 mg) was dropped on a PET substrate and then spun with varying spinning rates (1000–8000 rpm) in a spin coater, followed by curing in an oven under ~ 55 °C for ~ 16 h. The PDMS thickness was controlled by varying the spinning rate.

Then, bismuth telluride was deposited onto these various-thickness acrylate and PDMS interlayers (as well as a blank PET substrate for a control group) using DC magnetron sputtering at room temperature with an applied power of 0.25 kW on a three-inch Bi₂Te₃ target (99.999%, Mi-Net Technology Ltd.) under a vacuum of 1.8×10^{-4} mbar base pressure ($\approx 8.4 \times 10^{-4}$ mbar in 250 sccm argon flow) for 3 mins, in an Aerre Machines Vacuum R2R webcoater (see Fig. S1 b). Since the high-throughput R2R process cannot make very thick coating, the film thickness was controlled below 100 nm, as reported from our previous study [19].

2.2. Sample characterisation

The thickness of the acrylate layer and Bi—Te film were measured using a Veeco DekTak 6 M stylus profiler, which measured, in at least eight locations, the step height (using contact profilometry technique) between the film and the substrate made by masking the substrate with polyimide tapes. To determine the thickness of the PDMS layer, the mass difference was measured before and after deposition using a laboratory balance (Mettler Toledo), so the thickness of PDMS interlayer could be roughly calculated using the relation: mass = density (0.98 g/mL in this case) \times volume = density \times (the film thickness \times the substrate area).

Both tensile and buckling tests (Fig. 1) were conducted to investigate the in-plane stretching and bending forces during R2R manufacture and in wearable device operation. Tensile tests were performed in a Linkam Scientific TST350 using a 200 N load cell (using samples of a dog bone-like shape: width 10 mm \times length 20 mm with a semicircle of 2 mm radius in the middle at each side). The tensile velocity was fixed at 10 $\mu\text{m s}^{-1}$ and the sample thickness was varied, see Section 3.1. The dog-bone shape is used to concentrate the stress in the middle section and to avoid failure at the grips. Since the film is conductive and the substrate is insulating, cracking of the coating can be identified from the change of electrical resistance of the coating, hence an ohmmeter was used to measure the resistance of the film along the loading direction with a copper adhesive electrode (connected by silver paste). The buckling test was carried out using a rectangular sample (5 mm \times 37 mm) in an in-house custom system within the Oxford Seebeck testing apparatus, where the cold-side stage was moved at a speed of 0.3 mm s⁻¹ by a 24 V DC geared motor. The strain applied to the functional coating was affected by the displacement of the cold side which thus was accurately controlled according to a calculation method as reported in [20]. This model calculated the strain considering factors of the displacement, the sample thickness and length. Because the buckling test was built within the Oxford Seebeck system, an in situ Seebeck measurement can be acquired during buckling tests. In addition, an automated cycling of buckling was conducted for a number (50–140) of cycles.

Roughnesses of Bi—Te films and interlayer surfaces were characterised by AFM (atomic force microscope, Agilent 5400) using tips (NCHV-A, Bruker Ltd.) in tapping mode over six independent locations of 0.8 $\mu\text{m} \times 0.8 \mu\text{m}$. Images were processed (flattened and smoothed)

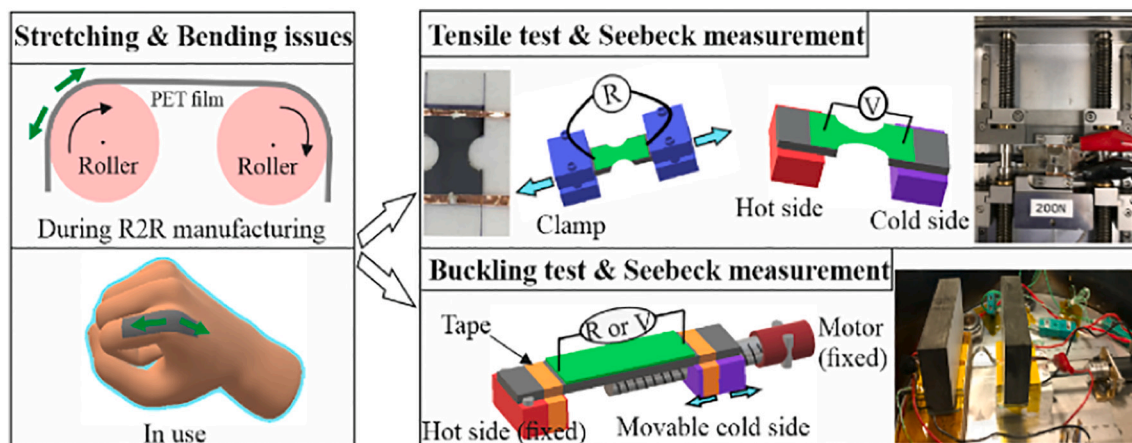


Fig. 1. Schematic diagrams of tensile and buckling setups. In the buckling test, the Bi—Te coated side is uppermost, and hence a tensile strain is induced on the coating.

using WSxM 5.0 Develop 9.0 software. The cracking of films was analysed using a 3D optical profilometer MicroXAM 5000B. The tensile strained samples were imaged after tensile tests (following material recovery), while the buckled samples were imaged in situ under bending strain.

An in-house custom Seebeck system was used to measure Seebeck coefficient (S) of Bi—Te film along the in-plane direction by applying temperature differences from 3 K to 62 K, with S determined by the ratio of an output voltage (ΔV) generated across the film surface to a temperature difference (ΔT). The fit line of ΔV vs ΔT had an $R^2 > 0.998$ for all samples. A variation of S was $<4.5\%$ obtained from three repeat measurements. The tensile-stretched specimen was measured after tensile tests (i.e. the strain released), while the buckled sample was measured in situ during buckling tests (i.e. under strain).

After tensile tests, the electrical resistivity (ρ) of a relaxed Bi—Te film held at room temperature was measured by a home-built van der Pauw system, using a Keysight B2901A. Four electrodes were made by silver paste at each corner of the sample. The variation of ρ over 5 measurements was $<5\%$. In terms of buckling tests, the sample shape was a standard rectangle thus the ρ can be directly calculated from the relation: resistivity = resistance \times area/length. Using this calculation method, the variation of ρ over four measurements was $<2\%$.

Power factor (PF) was then calculated from the product of S^2 and ρ^{-1} .

The sample-to-sample variation of Bi—Te film manufacture has been evaluated. The batch-to-batch variation is 4.4% in thickness, 3% in electrical resistivity and 1.5% in Seebeck coefficient from four independent batches.

3. Results and discussions

3.1. Film thickness and surface morphology

The thicknesses of the acrylate interlayers were manufactured in the range $0.4 (\pm 0.01) - 7.7 (\pm 0.09) \mu\text{m}$ and the PDMS coatings in the range $2.5 (\pm 0.01) - 16.8 (\pm 0.01) \mu\text{m}$ by controlling the amount of injected monomer and the spinning speed, respectively (Fig. S2 a). The Bi—Te film was sputtered to a thickness of $92 (\pm 6) \text{ nm}$ for all samples. These thicknesses can be used to calculate the strain applied to the film during buckling tests, using the model reported in [20]. The trends of strain with buckling displacement are shown in Fig. S2 b. The displacements of all samples are displayed in Table S1. The buckling strain was varied from 0.6–2% for Bi—Te deposited on PET with/without the thickest interlayers ($7.7\text{-}\mu\text{m}$ acrylate and $16.8\text{-}\mu\text{m}$ PDMS). The effect of thickness of interlayer was investigated under a fixed coating strain of 2%.

AFM images and root mean square roughness (RMSR) of the substrates (PET and PET with interlayers) and Bi—Te films on substrates are

shown in Fig. 2. RMSR of all substrates are in the range of 1–1.8 nm, with the interlayers observed to typically have slightly greater roughness. The constant surface roughness PDMS of various thicknesses indicates that the surface roughness of spin-coated PDMS ($\sim 1.6 \text{ nm}$, in a similar range as reported in [21]) is dominated by the curing process rather than the spinning speed (i.e. the coating's thickness). The acrylate layer is deposited via a flash-evaporation technique under vacuum, and the coating is seen to become rougher as the thickness increases as observed previously [22]. The surface topography of Bi—Te film shows a granular texture as expected from an island-growth mechanism [19] for room temperature sputtering onto polymer substrates. The RMSR of Bi—Te films grown on PET and acrylate substrates basically follows the trend of their substrate's roughness, while the Bi—Te film grown on PDMS presents a quite rough surface even though the substrate is smoother than some of the acrylate substrates. This could be attributed to (a) a migration of low-molecular-weight mass of PDMS (in a vacuum) under bombardments of sputtered ions; (b) a poor sticking coefficient of Bi—Te onto PDMS (the inherently weak adhesion forces between the metal and PDMS has already been reported [23,24]).

3.2. Tensile test

In the tensile test, there is no coating (either interlayer or Bi—Te layer) on the clamping region under the grips. This is to simulate the real situation of the wearable case or R2R: the stress is only directly applied to the PET substrate rather than the localised coating on top of PET in device structures. Hence, during the tensile test, the grips only clamp/stretch the PET sheet, which then the stretched PET causes strain in the coating. After the sample is clamped, the grips are slightly/precisely moved (by software control, $0.005 \mu\text{m s}^{-1}$) to put the sample at a 'just-flat' condition (i.e. just under tension) before the tensile test.

Tensile results of Bi—Te films on PET sheets with/without interlayers are shown in Fig. 3. The sample dimensions in the plane are constant for all samples, but the thickness varies. Hence, in this case, the sample stiffness κ , is proportional to, load \div (displacement \times sample thickness). The measured κ is taken from the slope of the linear portion of the load-displacement trace at low strain. For the PET sheet $\kappa = 1.088 \text{ N } \mu\text{m}^{-2}$ (see Fig. 3 a). After growing a Bi—Te film on the PET sheet, κ ($1.085 \text{ N } \mu\text{m}^{-2}$) does not change significantly, as would be expected of a thin, brittle layer despite its greater Young's modulus ($31\text{--}52 \text{ GPa}$ [25]) than PET (3.1 GPa [26]). Hence, for analysis of the stiffness, the influence of the very thin Bi—Te could be neglected.

The 'stiffness' of the composite, κ_c , made up of the PET substrate and the interlayer is given by:

$$\kappa_c d_c = d_{\text{PET}} \times \kappa_{\text{PET}} + d_{\text{interlayer}} \times \kappa_{\text{interlayer}} \quad (1)$$

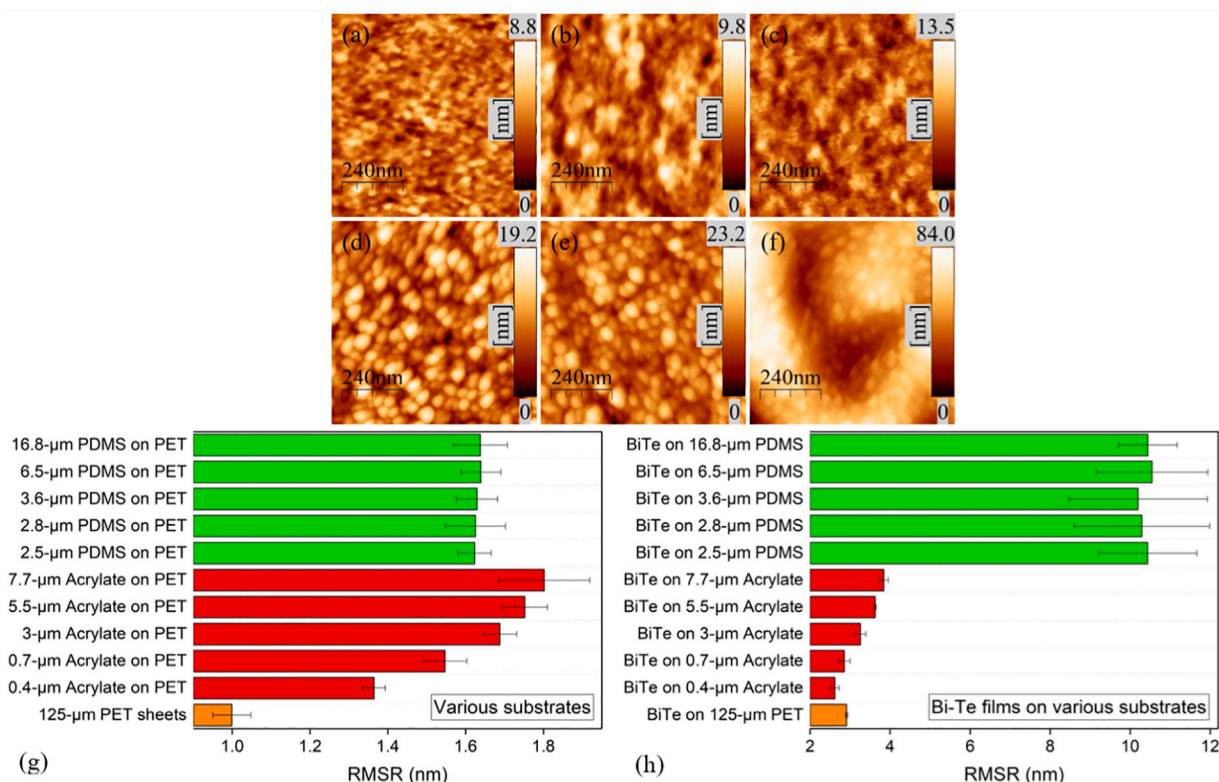


Fig. 2. AFM images of substrates (a) blank PET, (b) 0.4- μ m acrylate layer on PET, (c) 16.8- μ m PDMS layer on PET; and Bi—Te film grown on (a) (b) (c) corresponding to (d) (e) (f), respectively; RMSR of (g) PET substrates and interlayers coated on PET substrates; (h) Bi—Te film grown on different substrates. (The error bars in RMSR represent standard deviations from six AFM images: 0.8 μ m \times 0.8 μ m).

where d indicates the thickness of the layer, given the same in-plane film dimension and shape.

A 16.8- μ m thick PDMS coated on a 125- μ m thick PET has a measured κ of 0.96 N μ m⁻², and hence κ of PDMS can be calculated as 0.001 N μ m⁻². Similarly the κ of acrylate can be calculated from the measured κ_c (1.05 N μ m⁻²) of a film with a 7.7 \sim μ m thick acrylate coating to be 0.43 N μ m⁻². Thus the PET is found to be the stiffest material, and PDMS the most flexible with the ratio PET: acrylate: PDMS (1088: 430: 1) which is comparable to the ratio of materials modulus reported in the literature: 3.1 GPa [26]: 2 GPa [27]: 3.7 MPa [28] (i.e. 838: 541: 1). Fig. 3 a shows the failure strains and failure forces of the substrates, but by these strains the Bi—Te has been severely compromised, and so these substrate properties are not discussed further here.

A substantial rise in electrical resistance of the Bi—Te layer is seen (Fig. 3 b-d) at higher strains associated with cracking damage to the semiconductor. Electrical contacts were made to the Bi—Te close to the grips and the resistance of the Bi—Te film was measured in situ during tensile tests. The tracked electrical resistance of the ‘PET sample’ shows an apparent increase after a displacement of 0.15 μ m, and is changed by 800%, (2.7–0.3) \div 0.3, by a displacement of 0.3 μ m (i.e. \sim 2% tensile strain).

With interlayers, the point where the resistance of the sample is observed to rapidly increase is at a greater deformation (\sim 0.18 μ m) for the sample with the acrylate interlayer, and at a lesser deformation (\sim 0.03 μ m) for the sample with the PDMS interlayer. This could be due to the much higher roughness of the ‘PDMS sample’ which facilitates the formation of localised cracks.

Under a 0.3 μ m displacement, the resistance had substantially increased in all samples: by 800% for PET, but only 400% and 617% for the samples with an acrylate and PDMS interlayer, respectively, indicating that both interlayers could help to maintain the electrical performance of Bi—Te.

3.2.1. Change in morphology after tensile strain

During tensile tests, the substrate is elongated and the strain will be translated to the Bi—Te coating which may therefore crack under strain. Choice of the substrate's modulus is important for a brittle functional film grown on a polymer substrate [29]. Fig. 4 illustrates two possible mechanisms that could help to maintain the functional performance of Bi—Te: (a) a sliding phenomenon (i.e. the frictional sliding at an interface [30]) that would depend on the interfacial adhesion strength between a coating and the underlying layer [31]; (b) if an interlayer is deformable, there will be less strain on the coating on top of the interlayer than that on the bottom where the stress is applied to the substrate: a ‘shear lag’.

The morphological change in the Bi—Te film induced by tensile testing is investigated by white light interferometry, MicroXAM (Fig. 5). Samples are assessed after tensile tests following elastic recovery (i.e. MicroXAM imaging after the tensile strain is removed). This imaging will show large cracks through the thickness of the coating, but not interfacial cracking/slippage. Surface morphologies of the ‘PET sample’ and the ‘acrylate sample’ are similar while the ‘PDMS sample’ shows a completely different surface morphology (a typical nanocluster structure, similar to that observed in [24,32]). There is no noticeable change observed in the ‘PET sample’ until a tensile extension of 0.26 μ m, while Fig. 3 b suggests that the resistance of Bi—Te starts to change after only 0.15 μ m extension, hence, there could be cracks (e.g. nano size) formed on Bi—Te between 0.15 and 0.26 μ m extension that are not detectable by the MicroXAM. Under a 0.3- μ m extension, the ‘PET sample’ shows a high density of cracks perpendicular to the direction of stretching. Cracks are also observed for the ‘acrylate sample’ with a tensile extension of 0.26 μ m and become severe with respect to depth and crack density after applying a 0.3- μ m extension. Quite small cracks appear in the furrows (Fig. 5 f) of the ‘PDMS sample’ with a tensile extension of 0.26 μ m, and a clear/large/vertical crack is observed when the extension is 0.3 μ m. Again, the observed cracking point (tensile extension = 0.26 μ m, Fig. 5 e & f) for the ‘acrylate sample’ and the ‘PDMS sample’ is

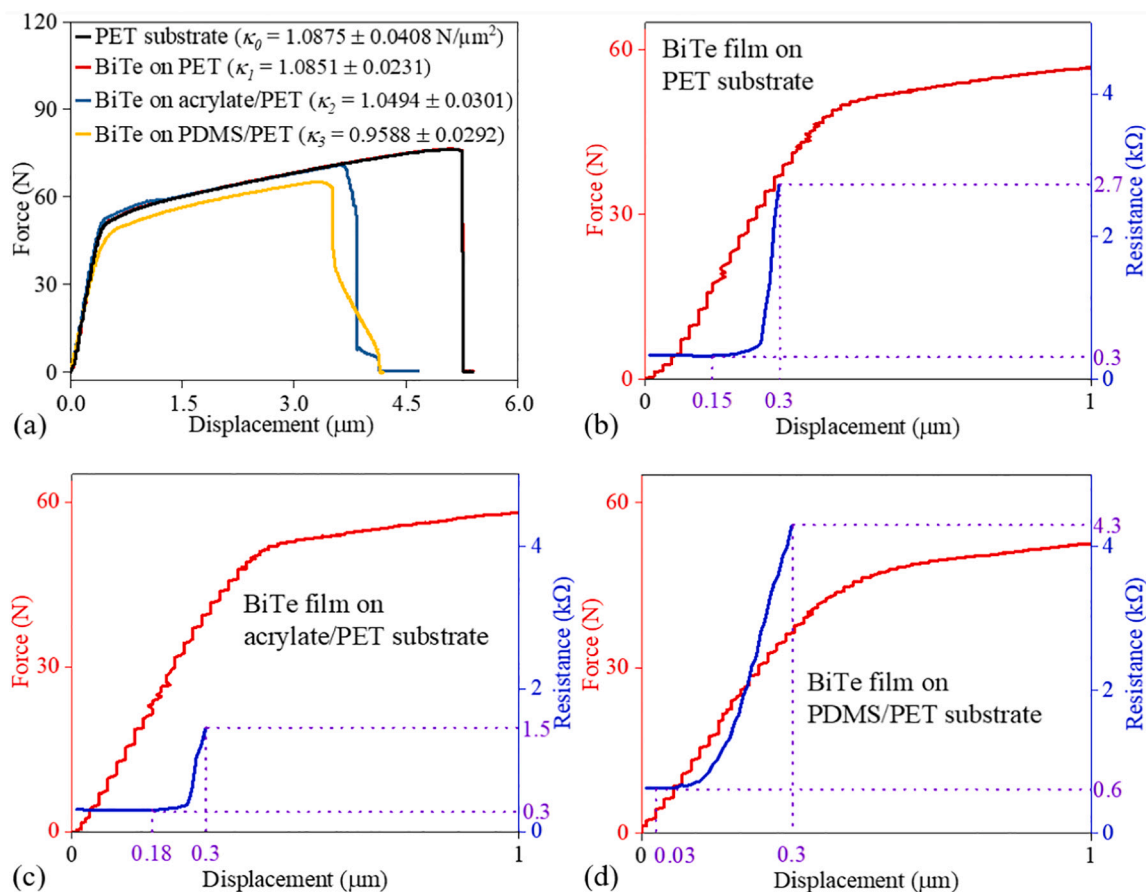


Fig. 3. (a) Tensile force-displacement curve of PET sheet, 7.7- μm acrylate + PET sheet, and 16.8- μm PDMS + PET each with a $\sim 90\text{-nm}$ Bi-Te coating; Plots of force and resistance against displacement for Bi-Te films on (b) PET sheet, (c) 7.7- μm acrylate + PET sheet, and (d) 2.5- μm PDMS + PET (where κ is calculated from the slope below $0.3 \mu\text{m}$ displacement, with standard deviation obtained from at least three samples. 0.15, 0.18, and $0.03 \mu\text{m}$ are the starting points of resistance to change).

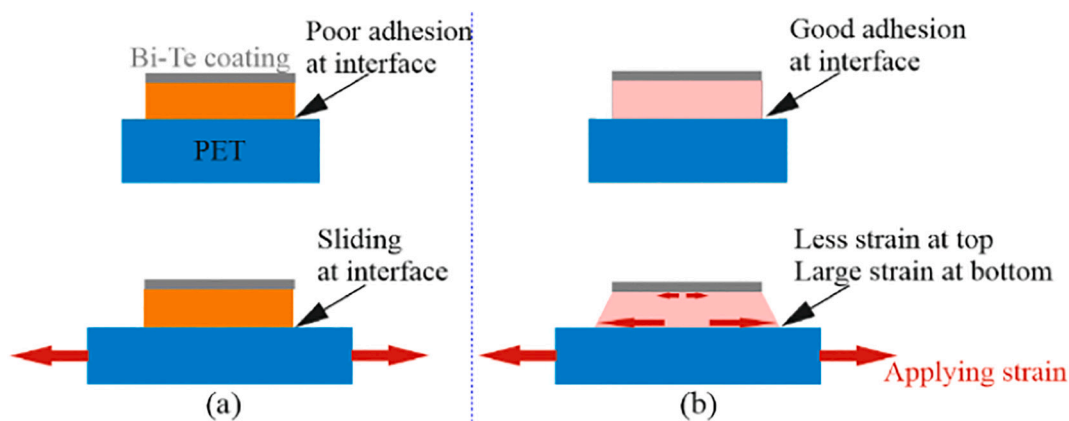


Fig. 4. Two mechanisms by which interlayers (in between PET and Bi-Te) may help maintain the Bi-Te coating under tension. (NB: this is the cross-section view and it does not represent the real thickness of these three layers, e.g. the bottom PET = $125 \mu\text{m}$, and the top Bi-Te = 92 nm).

greater than the strain at which electrical resistance begins to increase (0.18 or $0.03 \mu\text{m}$, Fig. 3 c & d). Comparing the morphology (Fig. 5) with the change in resistance (Fig. 3), it is clear that no cracks are observed for extensions in which the electrical resistance is constant, and the sample with observed cracks shows a very high resistance.

It can be observed that fewer cracks are formed in films with a thicker interlayer (see Fig. 5 h, j, k, and l: the 'acrylate samples'; Fig. 5 i, m, n, and o: the 'PDMS samples'), perhaps suggesting a contribution from the mechanism in Fig. 4 b. The decrease in the crack density with

the coating thickness has already been reported [33] due to a greater shear lag for the thicker coating. The shear lag allows the strain in the substrate to be locally accommodated by shearing of the interlayer. Thus samples with the greatest shear lag will have a lower density of (wider) cracks as the local strain around the cracked region can be accommodated by the interlayer. This analysis suggests that shear deformation of the interlayer is making a significant contribution, rather than the properties simply being controlled by interfacial slippage.

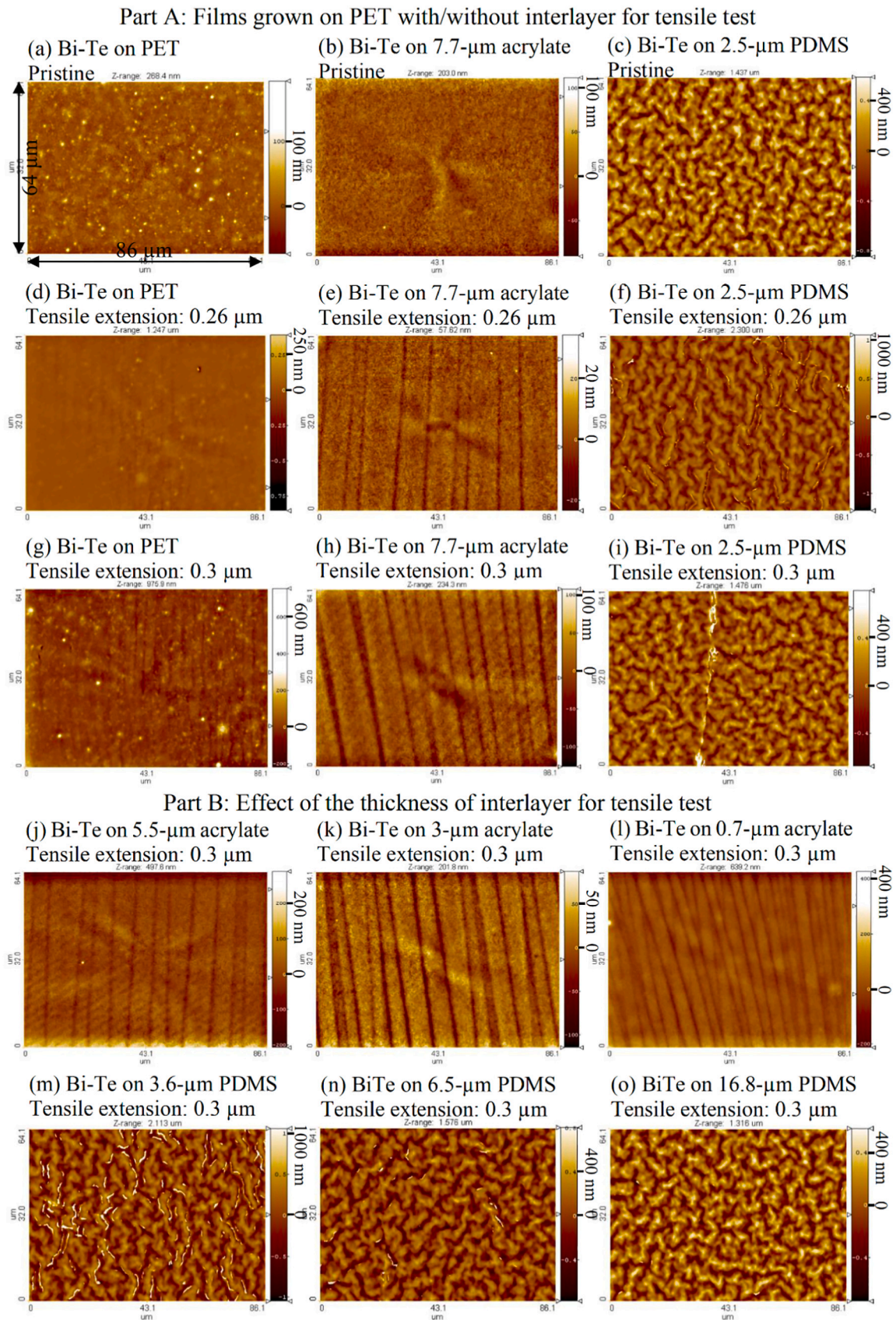


Fig. 5. MicroXAM images of after-tensile-strained Bi—Te films on PET sheets with/without interlayers. Bi—Te film grown: on PET with (a) 0, (d) 0.26 and (g) 0.3- μm tensile extension; on 7.7- μm acrylate/PET with (b) 0, (e) 0.26 and (h) 0.3- μm extension; on 2.5- μm PDMS/PET with (c) 0, (f) 0.26 and (i) 0.3- μm extension. A variation on interlayer thickness: (j–l) acrylate; (m–o) PDMS.

3.2.2. Changes in thermoelectric behaviours after tensile strain

The measurements in this section were conducted after the tensile stress was released from the samples. Fig. 6 shows the changes in ρ , S , and PF of Bi—Te films on PET as a function of extension (i.e. strain applied). The ρ , S and PF of unstrained Bi—Te film on PET sheets are $1.6 \text{ m}\Omega\cdot\text{cm}$, $67.5 \text{ }\mu\text{V K}^{-1}$ and $2.83 \times 10^{-4} \text{ W m}^{-1} \text{ K}^{-2}$, respectively. As the extension increases, S shows a slight decrease (e.g. $\sim 19\%$ for a $0.3\text{-}\mu\text{m}$ extension) while ρ increases significantly (e.g. $\sim 114\%$ for $0.3\text{-}\mu\text{m}$ extension), resulting in a significant decrease in PF (e.g. $\sim 70\%$ for $0.3\text{-}\mu\text{m}$ extension). This indicates that the change in PF is mainly dominated by the change in ρ . The rapid rise in ρ after a certain extension can be easily understood if it is associated with the onset of cracking. The start of cracking can impede carrier flow [34] due to fewer percolation paths for charge transport, while the mechanism by which cracks affect S is

still unclear. In theory, S is only dependent on the temperature difference applied between the cold side and hot side. Hence, (1) S should keep constant if cracking does not break all percolation paths; (2) If cracking breaks all paths, it becomes an open circuit (i.e. a failure in TE materials: no S); (3) If nano-size cracking forms an energy barrier that still allows high-energy carriers to pass, thus introducing a carrier filtering mechanism, and this would lead to an increase in S . All of these assumptions are inconsistent with the observation here (i.e. S decreases with cracking). Ou et al. [35] carried out a fatigue test for TE materials on polyimide sheets, and they observed micro-cracks formed on the surface as well as a slight decrease in S ($\sim 15\%$) after 60-h prolonged fatigue, but they concluded that this degradation in S was negligible. Zhang et al. [36] also found a slight decrease in S for TE materials with micro-cracks. Case et al. [37] reviewed studies about the effect of

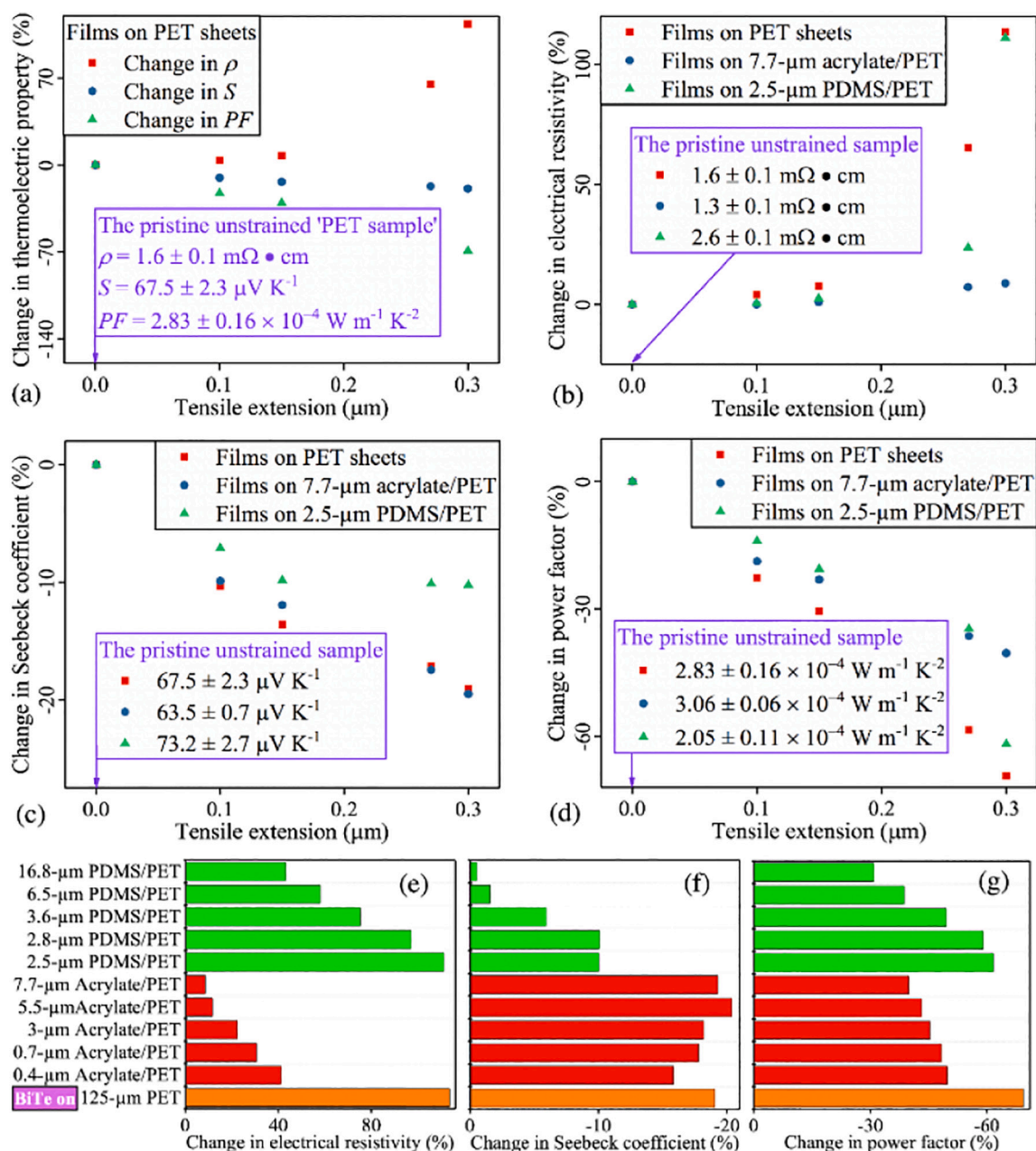


Fig. 6. (a) Changes in ρ , S and PF of Bi—Te film on PET under various strains (i.e. extension) after tensile test (samples relaxed); (b–d) Changes in ρ , S and PF of Bi—Te film on PET with/without interlayers under various strains; (e–g) Changes in ρ , S and PF of Bi—Te film on PET with various-thickness interlayers after stretching of $0.3 \text{ }\mu\text{m}$. (The numbers in the inset purple box are the average results from three measurements of S and five measurements of ρ). (For interpretation of the references to colour in this figure legend, the reader is referred to the web version of this article.)

cracking on TE performance, while there is still not a clear explanation on how cracks affect S .

Fig. 6 b-d shows the effect of interlayers on the change of TE performance compared to the unstrained sample. The absolute values for the unstrained samples are displayed in the inset table in Fig. 6 b-d. For the unstrained samples, there are differences in S and ρ for Bi—Te films grown on PET and interlayers, which could be attributed to the morphology of the Bi—Te on PET, acrylate, and PDMS (see Fig. 2). Other possible factors for the variation of Bi—Te grown on different substrates (e.g. stoichiometry or crystallinity of the Bi—Te) are not further analysed herein. In Fig. 6 b-d, it is clearly observed that interlayers help to avoid the changes in ρ and S , thus PF . The ‘PET sample’ shows the highest change in ρ under all extensions, which is likely due to a much greater density of cracks, as observed in Fig. 5. At these extensions, the resistance has risen moderately, so there are some paths for conduction either across apparent cracks or around cracks that do not cross the

entire width and thickness of the coating. Thus more cracks will tend to further limit the conductivity. The ‘acrylate sample’ shows a more effective ability to maintain ρ , while the ‘PDMS sample’ shows a better ability to maintain S .

For the ‘PDMS sample’ under tensile stress (Fig. 3 d), the resistance significantly increases at low strains (i.e. extensions: 0.03–0.3 μm) while the resistance in the ‘PET sample’ does not (Fig. 3 b), however, Fig. 6 b (after the tensile stress is released) suggests that the ρ of the ‘PDMS sample’ changes less than that in the ‘PET sample’ following the extensions of 0.1–0.26 μm . This indicates that under these extensions, the ‘PDMS sample’ could have a better ability to recover once the tensile stress is released. As can be seen in Fig. 5 f & i, only small cracks along the furrows are formed under extension $\leq 0.26 \mu\text{m}$, while a clear localised crack is formed under extension = 0.3 μm . The furrows should be attributed to the surface features of the PDMS, and it would be expected that these furrows would ‘open’ under stress and ‘close’ after the stress is

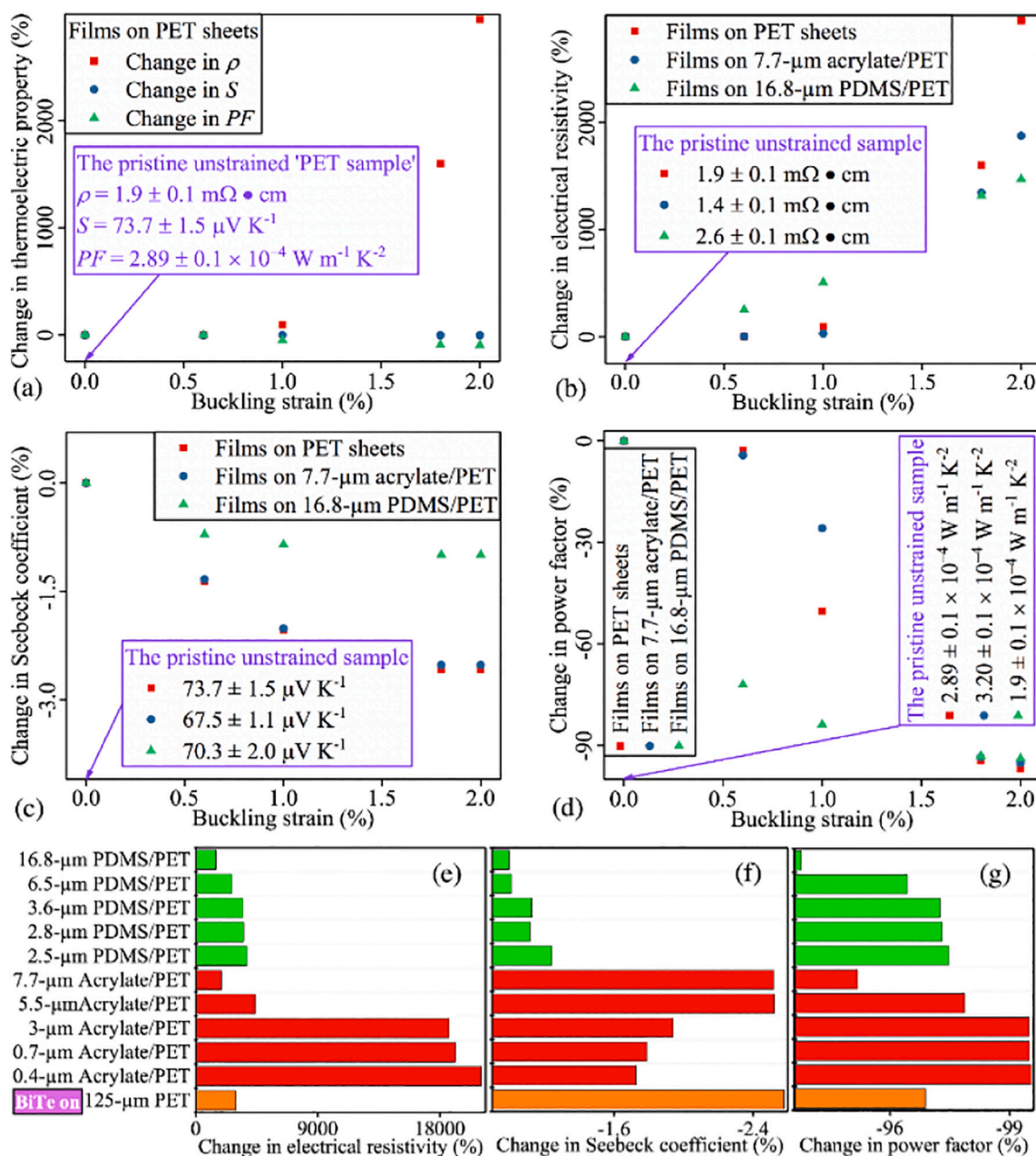


Fig. 7. (a) Changes in ρ , S and PF of Bi—Te film on PET under various strains during buckling test; (b-d) Changes in ρ , S and PF of Bi—Te film on PET with/without interlayers under various strains; (e-g) Changes in ρ , S and PF of Bi—Te film on PET with various-thickness interlayers during a buckling strain of 2%.

released. This recovery ability might explain the smaller change in ρ of the relaxed 'PDMS sample' compared to the 'PET sample' in Fig. 6 b, for extensions of 0.1–0.26 μm . It is noted that, under 0.3- μm extension, the 'PDMS sample' with a clear localised crack (Fig. 5 i) may not be able to recover so that the change in ρ is still significant (Fig. 6 b). This recovery ability could also be analysed from the observation of ρ during buckling test (i.e. under the buckling stress) in Fig. 7 b. During the buckling test, the furrows in the 'PDMS sample' will 'open', thus the change in ρ (Fig. 7 b) is much larger than others at the initial stage of buckling, which is consistent with the results of resistance during tensile stress in Fig. 3 d.

In terms of PF , although at greater strains (0.3- μm extension, Fig. 6 d) the acrylate interlayer protects the coating better (i.e. less change in PF) than the PDMS interlayer, under extensions $\leq 0.26 \mu\text{m}$ (Fig. 6 d), the PDMS interlayer shows a slightly better ability to maintain PF than the acrylate. This could be attributed to the better recovery ability of the PDMS interlayer.

The thickness effect of the interlayer is shown in Fig. 6 e–g. For both types of interlayers, a thicker interlayer shows less change in ρ , consistent with the fewer cracks observed in thicker layers (Fig. 5). As the thickness of interlayers increases, the change in PF decreases with the same trend of change in ρ . The observed comparable loss of performance between a 2.5- μm thick PDMS interlayer and the rather thicker 7.7- μm thick acrylate layer reflects the greater stiffness of the acrylate material, but both interlayers have some 'shear lag' effects as they both have a stiffness less than the substrate PET.

3.3. Buckling test

Unlike the tensile-test samples using a dog-bone shape, the buckling test was carried out using a rectangular sample (5 mm \times 37 mm). Again, the sample was clamped (taped) at a region of the PET without coating, hence, the Bi–Te film was under stress due to the deformation of the PET substrate to reflect the conditions during the R2R deposition and wearable application.

The displacement required to give a particular strain in the Bi–Te layer under buckling was calculated for each sample thickness. In Table S1, the calculated results illustrate how the thicker sample needs a smaller displacement to achieve the same strain on the upper surface of the film.

Both S and ρ were measured in situ while the sample was buckled. The resistance was measured then calculate to ρ by resistance \times width \times thickness \div length (NB: the sample width and length are same for all samples while the sample thickness varies according to the thickness of the interlayer). The previous section (tensile test) has suggested that the sample with a thicker interlayer behaves better. Hence, the 'PET sample' and samples with the thickest interlayer were imaged and characterised for thermoelectric performance.

3.3.1. Changes in morphology during buckling strain

To observe the morphology clearly, the sample was imaged (using MicroXAM) during buckling (see Fig. 8 b inset). The morphologies (see Fig. S3) are very similar to those shown in Fig. 5, although, as the sample is held under deformation for these images, the cracks appear more open.

Again, the 'PET sample' shows greater crack density compared with the 'acrylate sample' and the 'PDMS sample' under the same strain. Cracks become severe as the strain increases for all three sample types. As the thickness of the interlayer decreases, both the 'acrylate sample' and the 'PDMS sample' show an increasing number of much more severe cracks. These all are consistent with the analysis of the tensile-test sample in Fig. 5.

3.3.2. Changes in thermoelectric behaviours during buckling strain

Similarly as observed in the tensile test (Fig. 6 a), the PF decreases with increasing strain. The increase in ρ measured in situ during the buckling tests is substantially larger than that measured on a relaxed

sample following the tensile test. This could be due to the combined effects of i) the recovery of properties as the cracks are re-closed following sample relaxation and ii) the greater time (1–2 h) that the sample is held under strain while the in situ electrical measurements are made. This kind of cracking situation with time is similar to the result with cyclical buckling: in Fig. 8 a & b, by applying a 2% buckling strain to the 'PET sample', the resistance increases from 1.6 k Ω to 26.3 k Ω over the first cycle while it significantly increases to 306 k Ω after 50 cycles. Hence, with the buckling time or the number of buckling cycles or both, the cracking situation becomes more severe leading to an extremely large change in the electrical performance. In Fig. 7 b, the sample with the thickest (16.8 μm) PDMS interlayer behaves the best under 2% buckling strain indicating that the thick, low stiffness, PDMS interlayer has more ability to maintain the film performance, as expected from the previous analysis of the tensile-test samples.

In terms of the changes in S (Fig. 7 c), the 'PDMS sample' still behaves the best, as observed in the tensile-test results (Fig. 6 c), however, it is noted that the buckling-test sample has less change in S than the tensile-test sample. The change in PF depends on the changes in S and ρ . In the case of the buckling test, Fig. 7 d shows that the change in PF is dominated by the change in ρ .

Fig. 7 e, f, and g depict the effect of thickness of the interlayer. The S is changed by less than 3% so the change in ρ still dominates the results in PF . It is observed that only the sample with the thickest acrylate (95.2%) or PDMS (93.8%) layers possess the ability to maintain PF , in contrast to the 'PET sample' (96.9%). For the thinner samples, it is speculated that the interlayer could be delaminated under a buckling strain after a period of time, which makes the ρ worse than the pristine 'PET sample'.

In both the manufacturing process and the in-use wearable condition, samples will not permanently stay under strain, hence the cyclical-buckling test is also of interest.

3.3.3. Power measurements during cyclical buckling test

The effect of bending on the resistance of the Bi–Te strip (5-mm width \times 37-mm length) on PET sheet is shown in Fig. 8. Cycles of bending increase the resistance of Bi–Te samples, consistent with the observation in [10]. This is because the number of cracks increases with increasing bending cycles [26]. Under cyclical bending tests, there is negligible change in resistance under a buckling strain of 0.6%, and even 1%, which is within the elastic region for these materials (Fig. 3). Under 1.8% strain, the resistance can come back to the original level after 3 cycles, but after this, the resistance ($1.56 \pm 0.05 \text{ k}\Omega$) gradually increases and stabilises at $105 \pm 2 \text{ k}\Omega$ in ~ 50 cycles, which indicates that more cracks can develop over the initial cycles until there are no more cracks formed under this strain (i.e. an equilibrium of cracking condition under a specific strain). The situation is even worse when the buckling strain is 2% (3-cycle come-back, $306 \pm 6 \text{ k}\Omega$ at equilibrium).

As discussed in the introduction, a strain within 1% is of principal interest in both manufacturing and in-use situations. Fig. 8 a shows a $\sim 15\%$ increase in resistance under a strain of 1% after 80 cycles. To further study current and voltage outputs, a power measurement was conducted during cyclical bending tests, for samples with/without interlayers. The temperature difference applied was $14 \pm 0.3 \text{ K}$, simulating the real situation between the human body and the surroundings. Fig. 8 c, e, and g present current, voltage, and the calculated power (at 1.5 k Ω load, close to the internal resistance of the one-strip TEG to obtain the maximum power output [38]) during cyclical bending tests (1% strain), with a zoomed-in region in Fig. 8 d, f, and h, respectively. Due to the variation in thickness between samples, the buckling displacements are different. Each bending cycle (buckling + relaxing) requires 106, 100, and 96 s to apply an equivalent strain (1%), for the 'PET', acrylate, and PDMS samples, respectively. The initial variation in current and voltage (i.e. initial non-bending output at equilibrium) for the 'PET, acrylate, and PDMS samples' is due to the slight variation in performance of Bi–Te film grown on different substrates. In terms of current output

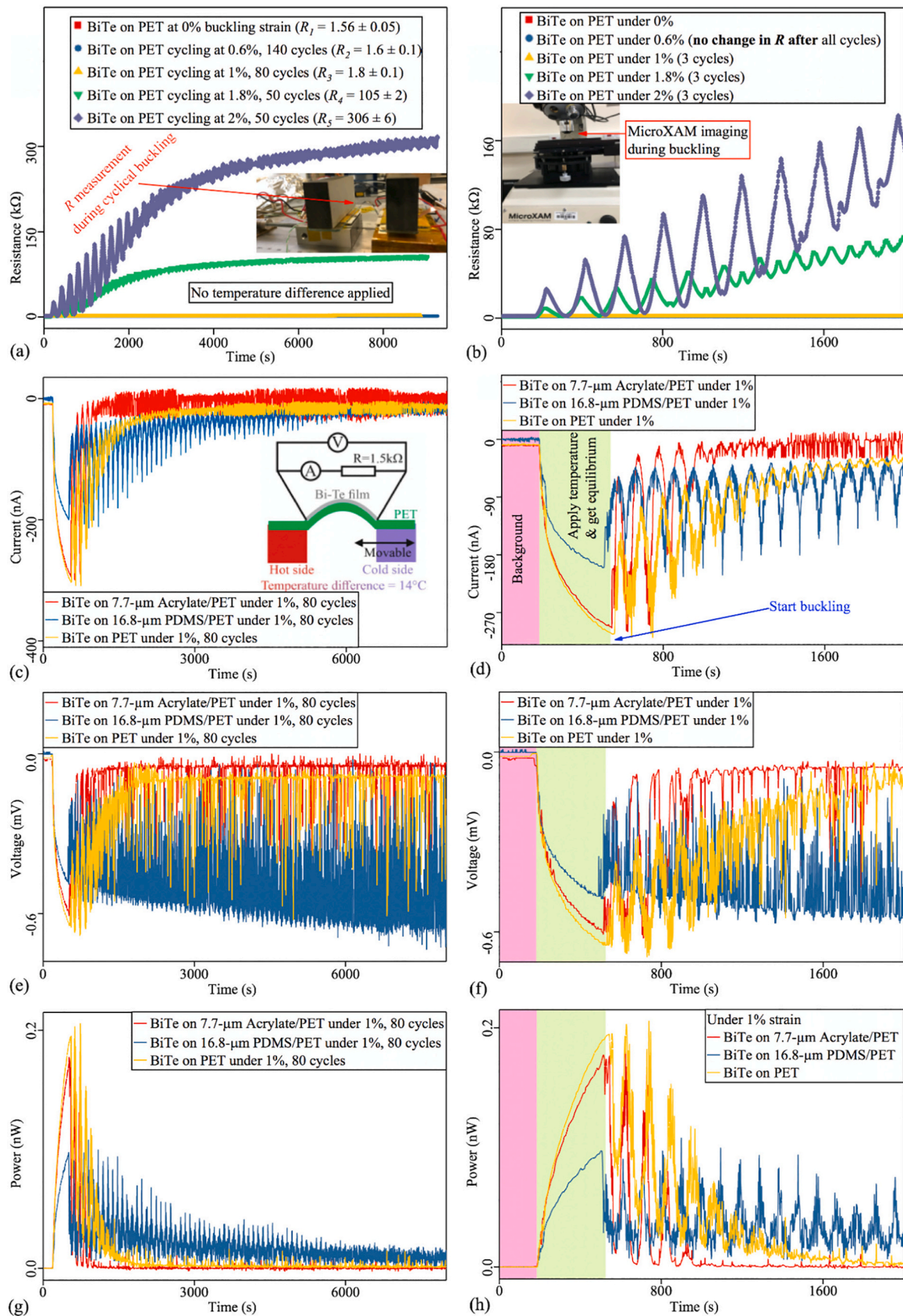


Fig. 8. (a) Resistance measurement for Bi-Te films grown on PET sheets under various buckling strains in cycling fatigue testing; (c) Current, (e) Voltage and (g) Power measurements, taken with a temperature difference of 14 K, of Bi-Te films on PET substrates (strip: 5-mm width \times 37-mm length) with/without interlayers in cycles of 1%-strain buckling tests. (b, d, f, h) are zoomed-in regions from (a, c, e, g), respectively.

(Fig. 8 d), the 'acrylate sample' failed (i.e. zero current output) at around 1000 s (4 cycles), the 'PET sample' almost failed at around 2000 s (14 cycles), whereas the 'PDMS sample' still worked after 8000 s (80 cycles). This is also the case for voltage output, and thus the power calculated from the measured current and voltage. As can be seen in Fig. 8 g, the 'PDMS sample' has a stable power output between 6000 and 8000 s (~ 0.015 nW). This is consistent with the superior recovery ability observed in the previous analysis for the samples with PDMS interlayers in both tensile and buckling tests. Overall, the cyclical fatigue behaviour of the samples without the interlayer, or with the acrylate interlayer is very poor because of its poor recovery capability, while the PDMS interlayer can improve the cyclical fatigue significantly and still work after 80 cycles of buckling tests.

4. Conclusion

An experimental study was carried out to investigate the mechanical stability of ~ 90 -nm thick Bi—Te film grown on flexible polymer sheets (~ 125 μm PET), and two types of interlayers (0.4–7.7 μm -thick acrylate and 2.5–16.8 μm -thick PDMS) were proposed to improve the mechanical resilience. To simulate a real situation during operation and manufacture processing, both tensile and buckling strains were applied to the substrate, inducing strains in the TE coating. The thermoelectric performance was measured after the tensile strain and during buckling strain. In addition, a cyclical-bending test was carried out in cycles of buckling tests, meanwhile, the power output of a 5 mm \times 37 mm strip was obtained through measuring voltage and current in an Ohm's circuit.

After tensile strain (allowing a recovery process when the tensile stress is released), a thicker interlayer (acrylate or PDMS) shows an ability to ease the changes in ρ and S , and thus PF , because they help to avoid the formation of cracks suggested to be due to shearing of the interlayer retarding the strain applied to the more brittle Bi—Te.

During buckling strain, since there is no recovery process in these experiments, the cracks stay open during observation and testing. Samples with acrylate interlayers still show an ability to maintain thermoelectric performance, while samples with PDMS layers show a larger change in resistivity once the strain is applied, potentially reflecting the different morphology of the Bi—Te on the PDMS. Considering the small change observed in tensile strained samples with PDMS layers, there appears to be a good ability of PDMS samples to recover their properties once the load is released, and this is confirmed in the subsequent cyclical-bending test. Again, a thicker interlayer is preferred because, without a recovery process, only samples with the thickest interlayers in this case maintain their performance during strain. In cyclical-bending tests, the sample with PDMS shows much better recovery ability than others.

CRediT authorship contribution statement

Xudong Tao: Conceptualization, Methodology, Investigation, Writing – original draft. **Kai Zhang:** Methodology. **Bryan W. Stuart:** Methodology, Writing – review & editing. **Hazel E. Assender:** Supervision, Writing – review & editing.

Declaration of competing interest

The authors declare that they have no known competing financial interests or personal relationships that could have appeared to influence the work reported in this paper.

Acknowledgements

This study was supported by the Engineering and Physical Sciences Research Council [grant number EP/M015173/1] via the Wearable and flexible technologies enabled by advanced thin-film manufacture and

metrology Collaboration. PET substrates were kindly supplied by DuPont Teijin films. The authors would like to acknowledge Oxford Semiconductor and Silicon Photovoltaics Group, and Oxford Materials Characterisation Services for equipment access. We would like to especially thank to Dr. Colin Johnston and Mr. Richard Turner for technical assistance.

Appendix A. Supplementary data

Supplementary data to this article can be found online at <https://doi.org/10.1016/j.surfcoat.2022.128167>.

References

- [1] Q. Li, M. Deng, S. Zhang, D. Zhao, Q. Jiang, C. Guo, Q. Zhou, W. Liu, Synergistic enhancement of thermoelectric and mechanical performances of ionic liquid LITFSI modulated PEDOT flexible films, *J. Mater. Chem. C* 7 (2019) 4374–4381.
- [2] D. Kim, J.A. Rogers, Stretchable electronics: materials strategies and devices, *Adv. Mater.* 20 (2008) 4887–4892.
- [3] Y.S. Jung, M.H. Jeong, D.H. Jeong, S.B. Kang, J. Kim, F. Kim, K. Lee, J.S. Son, J. M. Baik, K.J. Choi, Wearable solar thermoelectric generator driven by unprecedentedly high temperature difference, *Nano Energy* 40 (2017) 663–672.
- [4] S.J. Kim, J.H. We, B.J. Cho, A wearable thermoelectric generator fabricated on a glass fabric, *Energy Environ. Sci.* 7 (2014) 1959–1965.
- [5] M. Culebras, K. Choi, C. Cho, Recent progress in flexible organic thermoelectrics, *Micromachines* 9 (2018) 638.
- [6] Z. Liu, G. Chen, Advancing flexible thermoelectric devices with polymer composites, *Adv. Mater. Technol.* 5 (2020), 2000049-n/a.
- [7] M.H. Jeong, A. Sanger, S.B. Kang, Y.S. Jung, I.S. Oh, J.W. Yoo, G.H. Kim, K.J. Choi, Increasing the thermoelectric power factor of solvent-treated PEDOT:PSS thin films on PDMS by stretching, *J. Mater. Chem. A* 6 (2018) 15621–15629.
- [8] A.B. Zhang, B.L. Wang, J. Wang, J.K. Du, C. Xie, Effect of cracking on the thermoelectric conversion efficiency of thermoelectric materials, *J. Appl. Phys.* 121 (2017) 45105.
- [9] Y. Liu, B.L. Wang, C. Zhang, Thermoelastic behavior of a thermoelectric thin-film attached to an infinite elastic substrate, *Philos. Mag.* 97 (2017) 43–57.
- [10] M.J. Zhuo Cao, R.N. Tudor, S.P. Beeby Torah, Screen printable flexible BiTe-SbTe-based composite thermoelectric materials on textiles for wearable applications, *TED* 63 (2016) 4024–4030.
- [11] K. Singkaseli, A. Sakulkalavek, R. Sakdanuphab, Effects of annealing temperature on the structural, mechanical and electrical properties of flexible bismuth telluride thin films prepared by high-pressure RF magnetron sputtering, *ANSN* 8 (2017) 350021–350027.
- [12] D. Kong, W. Zhu, Z. Guo, Y. Deng, High-performance flexible Bi₂Te₃ films based wearable thermoelectric generator for energy harvesting, *Energy* 175 (2019) 292–299.
- [13] T. Baëtens, E. Pallechi, V. Thomy, S. Arscott, Cracking effects in squashable and stretchable thin metal films on PDMS for flexible microsystems and electronics, *Sci. Rep.* 8 (2018), 9492, 17.
- [14] C. Dagdeviren, P. Joe, O.L. Tuzman, K. Park, K.J. Lee, Y. Shi, Y. Huang, J.A. Rogers, Recent progress in flexible and stretchable piezoelectric devices for mechanical energy harvesting, sensing and actuation, *Extreme Mech. Lett.* 9 (2016) 269–281.
- [15] X.D. Wang, S.A. Meguid, On the electroelastic behaviour of a thin piezoelectric actuator attached to an infinite host structure, *Int. J. Solids Struct.* 37 (2000) 3231–3251.
- [16] X. Tao, K. Zhang, D. Gregory, J. Liu, H.E. Assender, Device optimization and large-scale roll-to-roll manufacturability of flexible thin-film thermoelectric generators, <sb:contribution><sb:title>Energy Technol. (Weinheim</sb:title></sb:contribution><sb:host><sb:issue><sb:series><sb:title>Germany</sb:title></sb:series></sb:issue></sb:host> 9 (2021) n/a.
- [17] Z. Ding, G.A.W. Abbas, H.E. Assender, J.J. Morrison, S.G. Yeates, E.R. Patchett, D. M. Taylor, Vacuum production of OTFTs by vapour jet deposition of dinaphtho [2,3-b:2',3'-f]thieno[3,2-b]thiophene (DNTT) on a lauryl acrylate functionalised dielectric surface, *Org. Electron.* 31 (2016) 90–97.
- [18] T. Cosnahan, A.A.R. Watt, H.E. Assender, Flexography printing for organic thin film transistors, *Mater.Today: Proc.* 5 (2018) 16051–16057.
- [19] X. Tao, K. Wan, J. Deru, E. Bilotti, H.E. Assender, Thermoelectric behaviour of Bi-Te films on polymer substrates DC-sputtered at room-temperature in moving web deposition, *Surf. Coat. Technol.* 385 (2020), 125393.
- [20] Z. Chen, B. Cotterell, W. Wang, The fracture of brittle thin films on compliant substrates in flexible displays, *Eng. Fract. Mech.* 69 (2002) 597–603.
- [21] M. Bračić, T. Mohan, R. Kargl, T. Griesser, S. Hribernik, S. Köstler, K. Stana-Kleinschek, L. Fras-Zemljic, Preparation of PDMS ultrathin films and patterned surface modification with cellulose, *RSC Adv.* 4 (2014) 11955.
- [22] Carmen Alonso Herr, Hazel Assender, Roll-to-roll Vacuum Deposition of Organic Thin Films Followed by In-line Curing, Oxford University, 2020. Thesis.
- [23] D. Koh, A. Wang, P. Schneider, B. Bosinski, K.W. Oh, Introduction of a chemical-free metal PDMS thermal bonding for fabrication of flexible electrode by metal transfer onto PDMS, *Micromachines* 8 (2017) 280.
- [24] B. Osmani, H. Dehyle, F.M. Weiss, T. Töpfer, M. Karapetkova, V. Leung, B. Müller, Morphology and conductivity of Au films on polydimethylsiloxane using (3-

- mercaptopropyl)trimethoxysilane (MPTMS) as an adhesion promoter 9798, 2016, 11.
- [25] T. Lai, K. Wang, T. Fang, C. Huang, Effect of the interface on the mechanical properties and thermal conductivity of bismuth telluride films, *Mater.Res.Express* 5 (2018) 26408.
- [26] J. Hsu, C. Lee, B. Wen, P. Huang, C. Xie, Experimental and simulated investigations of thin polymer substrates with an indium tin oxide coating under fatigue bending loadings, *Materials (Basel, Switzerland)* 9 (2016) 720.
- [27] S.M.M.A. Rahman, A.I. Mustafa, M.A. Khan, Jute reinforced polypropylene composite: effect of surface pretreatment by photocuring with acrylic monomers, *J. Reinf. Plast. Compos.* 28 (2009) 1733–1745.
- [28] Z. Wang, A.A. Volinsky, N.D. Gallant, Crosslinking effect on polydimethylsiloxane elastic modulus measured by custom-built compression instrument, *J. Appl. Polym. Sci.* 131 (2014) n/a.
- [29] R. Chen, K. Pan, H. Lin, N. Wei, F. Zuo, Ductility of thin metal film on a polymer substrate for stretchable electronics, *Mater. Res. Innov.* 19 (2015) S8–S272.
- [30] R.R. Collino, N.R. Philips, M.N. Rossol, R.M. McMeeking, M.R. Begley, Detachment of compliant films adhered to stiff substrates via van der Waals interactions: role of frictional sliding during peeling, *J. R. Soc. Interface* 11 (2014) 20140453.
- [31] Z. Chen, K. Zhou, X. Lu, Y. Lam, A review on the mechanical methods for evaluating coating adhesion, *Acta Mech.* 225 (2014) 431–452.
- [32] Y. Zhang, S. Yu, M. Chen, P. Cai, H. Zhou, Impurity induced wrinkling patterns in metal films deposited on soft elastic substrates, *Surf. Rev. Lett.* 24 (2017) 1750034.
- [33] Y. Leterrier, J. Andersons, Y. Pitton, J.-E. Manson, Adhesion of silicon oxide layers on poly(ethylene terephthalate). II: effect of coating thickness on adhesive and cohesive strengths, *J. Polym. Sci. B Polym. Phys.* 35 (1997) 1463–1472.
- [34] H. Lee, S.J. Han, R. Chidambaram Seshadri, S. Sampath, Thermoelectric properties of in-situ plasma spray synthesized sub-stoichiometry $\text{TiO}_2\text{--x}$, *Sci. Rep.* 6 (2016) 36581.
- [35] C. Ou, A.L. Sangle, T. Chalklen, Q. Jing, V. Narayan, S. Kar-Narayan, Enhanced thermoelectric properties of flexible aerosol-jet printed carbon nanotube-based nanocomposites, *APL Mater.* 6 (2018) 96101–96108.
- [36] L. Zhang, A. Grytsiv, B. Bonarski, M. Kerber, D. Setman, E. Schafner, P. Rogl, E. Bauer, G. Hilscher, M. Zehetbauer, Impact of high pressure torsion on the microstructure and physical properties of $\text{Pr}_{0.67}\text{Fe}_3\text{CoSb}_{12}$, $\text{Pr}_{0.71}\text{Fe}_{3.5}\text{Ni}_{0.5}\text{Sb}_{12}$, and $\text{Ba}_{0.06}\text{Co}_4\text{Sb}_{12}$, *J. Alloys Compd.* 494 (2010) 78–83.
- [37] E. Case, Thermal fatigue and waste heat recovery via thermoelectrics, *J. Electron. Mater.* 41 (2012) 1811–1819.
- [38] D. Enescu, Thermoelectric energy harvesting: basic principles and applications, in: *Green Energy Advances*, 2019.